EPTT 2024
Escola de Primavera de Transição e Turbulência

ABCM
Associação Brasileira de Engenharia e Ciências Mecânicas

EPTT2024-0027
ON THE EFFECT OF TURBULENCE MODELING ON THE HEMODYNAMICS OF INTRACRANIAL ANEURYSMS

Marcella Pereira de Almeida Dell'Avanzi
São Paulo State University (UNESP), School of Engineering, Bauru, São Paulo, Brazil
marcella.avanzi@unesp.br

José Luiz Gasche
São Paulo State University (UNESP), School of Engineering, Ilha Solteira, São Paulo, Brazil
jose.gasche@unesp.br

Heitor Temporim Ribeiro
São Paulo State University (UNESP), School of Engineering, Bauru, São Paulo, Brazil
heitor.ribeiro@unesp.br

Iago Lessa de Oliveira
São Paulo State University (UNESP), School of Engineering, Bauru, São Paulo, Brazil
iago.oliveira@unesp.br

Abstract. *Intracranial aneurysms (IAs) are dilations in the cerebral arteries, which can cause great danger if they rupture, causing intracranial hemorrhage and possibly leading to the death of the patient — IAs have a high mortality rate of up to 50 %. Rupture, however, is difficult to predict and, currently, surgical procedures also present risks for the patient. Numerical simulations of the flow within IAs have been widely used to study them due to the connection between hemodynamics and the initiation, growth and rupture of aneurysms, being the wall shear stress and the oscillatory shear index on the artery wall inner surface the main causes of evolution of an aneurysm. When using numerical simulations to solve this problem, adequate flow models are important and one of the most used hypotheses is that the flow is laminar, due to its low values of the Reynolds number. However, some studies indicate that transition to turbulence may occur inside the aneurysm due to the transient nature of the flow. In this context, it is important to check which turbulence models could be used to more adequately predict the wall shear stress in cases where transition occurs, which is the goal of this work. We numerically simulated the flow, using OpenFOAM®, inside an aneurysm case available in the Aneurisk repository using Computational Fluid Dynamics assuming, first, laminar flow regime, and with the k-ω SST and k_T-k_L-ω models by assuming that transition occurred. The results for wall shear stress and the oscillatory shear index were analyzed, indicating that the assumption of turbulence inside the aneurysm is indeed small.*
Keywords: *Intracranial aneurysms, Turbulence, Computational Fluid Dynamics, Wall shear stress*

1. INTRODUCTION

Intracranial aneurysms (IAs) are pathological dilatations in the vascular system occurring in the arteries that reach the brain, more commonly found in the bifurcations of that vascular tree, but also laterally to those arteries. It is a dangerous disease with up to 50 % mortality rate in case of rupture (Vlak *et al.*, 2013; Saqr *et al.*, 2019). The rupture event is hard to predict and the currently available treatments also pose risk to patients, leaving physicians with a tough decision about whether to treat or not a particular patient. Hence, more reliable metrics to predict the rupture event have occupied researchers for the past two decades and a possible path to find those metrics is to understand the progression of the disease leading to the rupture. Part of that research on the subject employed numerical tools, such as Computational Fluid Dynamics (CFD) (Liang *et al.*, 2019), because it is widely accepted today that IAs are acquired lesions related to the interaction between the hemodynamic environment in the aneurysm lumen and its wall. Currently, the practical use of numerical techniques to assess the likelihood of IA rupture is a debated topic in the literature (Kallmes, 2012; Cebral and Meng, 2012).

Laminar flow is the almost universal assumption about flow in cerebral arteries and in intracranial aneurysm, as the flow Reynolds number in those arteries varies in a range of 300–1000, a range that theoretically would guarantee laminar flow, based on classical results of the flow in pipes. However, the unsteady nature of this flow can cause it to transition into the turbulent regime. This is especially true inside an aneurysm geometry as suggested by some works. (Tupin *et al.*, 2020), for example, indicated a transition to the turbulent regime in an ideal model of aneurysmal flow with Reynolds numbers as low as 300. This potential transition inside intracranial aneurysms was investigated numerically by other works (Valen-Sendstad *et al.*, 2011; Jain *et al.*, 2016; Khan *et al.*, 2021). Valen-Sendstad *et al.* (2011), for example, using direct numerical simulation (DNS) verified an increase in the turbulent kinetic energy of the flow in a case of saccular aneurysm close to the moment of peak systole. The authors also8 found that the flow relaminarizes after this peak, indicating the strong influence time in the flow regime

The transition to turbulence in intra-aneurysmal flow would have an important impact on aneurysm research because the wall shear stress (WSS) and the oscillatory shear index (OSI) levels essentially depend on the flow regime (Poelma *et al.*, 2015). Hence, the WSS, for example, an important hemodynamic parameter related to aneurysm onset, growth and ruptured, in the aneurysm wall in numerical studies performed under the hypothesis of laminar flow would be underestimated. In this context, the goal of this work is to further understand the influence of turbulence inside aneurysmal flow by assessing the effect of using different turbulence models to numerically predict the WSS and OSI in its lumen wall compared to a laminar-flow assumption.

2. NUMERICAL METHODOLOGY

2.1 Sample Selection and Geometry Preparation

We selected two patient-specific vascular geometries, one harboring a lateral IA from a 26-year-old patient with and the other a bifurcation IA from a 74-year-old patient, available in the *Aneurisk* repository, which provides a set of 100 cases under the *Creative Commons BY-NC 3.0.* license. The two geometries used correspond to cases C0005 and C0038 of the repository. This selection was based on the different flow patterns that both types of aneurysms may present. Lateral cases present recirculation flow whereas the bifurcation case was selected due to the flow jet from the internal carotiod artery impinging on the aneurysm wall. This bifurcation case was a candidate to higher velocity magnitudes inside the aneurysm and, thus, to exhibit transition to turbulence. Furthermore, both cases are located at the internal carotid artery with inlet diameter of the lateral case of 3.2 mm and the bifurcation one with 5.5 mm, respectively.

2.2 Physical and Mathematical Modeling

Blood was assumed to be a Newtonian fluid with kinematic viscosity of approximately 4×10^{-6} m^2/s (Isaksen *et al.*, 2008). We numerically solved for the flow in the vascular geometries assuming three models: first, assuming a laminar flow regime in the entire geometry; second, using a fully-turbulent flow model and a transition to turbulence model. In the case of laminar flow assumption, both the continuity and Navier-Stokes equations were then numerically solved with the same as presented in a work by our group (Oliveira *et al.*, 2021).

By assuming the hypothesis of fully turbulent flow inside the aneurysm sac, the Reynolds-averaged Navier-Stokes equations were numerically solved with turbulence modeled with the *k*-ω SST closure model. In terms of the average kinematic quantities of the flow, the continuity equation is written as:

$$\nabla \bullet \overline{\boldsymbol{v}} = 0\,, \tag{1}$$

and the momentum equation is written as follows:

$$\frac{\partial \overline{\boldsymbol{v}}}{\partial t} + \nabla \bullet (\overline{\boldsymbol{v}}\overline{\boldsymbol{v}}) = -\frac{1}{\rho}\nabla \overline{p} + \nu \nabla^2 \overline{\boldsymbol{v}} + \frac{1}{\rho}\nabla \bullet \boldsymbol{\tau}^R\,, \tag{2}$$

where ν is the kinematic viscosity, $\overline{\boldsymbol{v}}\ \overline{p}$ are the mean velocity and mean pressure; $\boldsymbol{\tau}^R$ is the Reynolds stress tensor, which, under the Boussinesq's hypothesis, is:

$$\boldsymbol{\tau}^R = \rho \nu_{\mathrm{t}} \left[\nabla \overline{\boldsymbol{v}} + (\nabla \overline{\boldsymbol{v}})^{\mathrm{T}} \right]\,, \tag{3}$$

where ν_{t} is the turbulent kinematic viscosity. The *k*-ω SST was chosen as it was already used to model pulsatile turbulent flows (Scotti and Piomelli, 2002). Additionally, it has been developed to adequately predict recirculations in flows that have adverse pressure gradients, which may occur in the complex network of vessels and inside the aneurysm sac. It introduces two additional transport equations to close the system formed by Eqs. (1) and (2). Assuming the case of

incompressible and unsteady flow, the equation for the turbulent kinetic energy, k:

$$\frac{\partial k}{\partial t} + \nabla \bullet (\overline{\boldsymbol{v}} k) = \nabla \bullet \left[\left(\nu + \frac{\nu_\mathrm{t}}{\sigma_k} \right) \nabla k \right] + P_k - \beta^* k\omega \tag{4}$$

and for the turbulence frequency, ω:

$$\frac{\partial \omega}{\partial t} + \nabla \bullet (\overline{\boldsymbol{v}} \omega) = \nabla \bullet \left[\left(\nu + \frac{\nu_\mathrm{t}}{\sigma_\omega} \right) \nabla \omega \right] + Q^\omega \,, \tag{5}$$

where ν_t is the kinematic eddy viscosity, σ_k and σ_ω are the Prandtl numbers of the turbulent kinetic energy and the turbulence frequency are the effective kinematic viscosities of each variable; P_k is the rate of production of turbulent kinetic energy. For the sake of space, we summarized the rate of production, dissipation and cross-diffusion terms of the equation for ω into the term Q^ω. A detailed summary of this turbulence model, with details of the mathematical forms of the source terms in Eqs. (4) and (5), can be found in classical references such as Versteeg and Malalasekera (2007).

For the transition model, we selected the three-equation transition model, known as the k_T-k_L-$\boldsymbol{\omega}$ transition model. It is based on the $k-\omega$ turbulence model, but introduces a new transport equation for the laminar kinetic energy, k_L, which represents fluctuations in the flow before transition. The transition process is characterized by the transfer of energy from laminar kinetic energy to turbulent kinetic energy, k_T, associated with fluctuations characteristic of a fully turbulent flow. For the sake of space, the transport equations for k_T, k_L, and the specific dissipation rate, ω, in this model will not be included here, but can be found in Walters and Cokljat (2008).

Boundary Conditions

Regarding the flow boundary conditions for the average kinematic quantities, at the flow inlet (see Fig. 1a), a time varying pulsatile velocity profile was imposed, varying spatially according to the fully-developed laminar flow in a pipe:

$$\boldsymbol{v}_{inlet}(r,t) = 2\frac{q_a(t)}{A_{inlet}} \left[1 - \frac{4r^2}{{d_{pa}}^2} \right] \,, \tag{6}$$

where A_{inlet} is the cross-sectional area of the inlet artery, d_{pa} is its inner diameter, and r is the radial coordinate of the circular inlet section — an artificial circular-section extension, with a length equal to twice the diameter d_{pa}, is added to the artery inlet to impose this inlet flow condition. The blood flow rate, $q_a(t)$, corresponding to the flow pulse from the beginning of systole until the end of the diastole, was obtained by multiplying a normalized flow rate by the mean blood flow rate in the internal carotid artery (ICA) reported by Zarrinkoob *et al.* (2015). For the bifurcation case, the normalized waveform was taken from Hoi *et al.* (2010) that measured it for older adults (mean age 68 $\pm$ 8 years) and for the lateral case we used the normalized waveform measured by Ford *et al.* (2005) for young adults (mean age 28 $\pm$ 7 years) (the resulting profiles are shown in Fig. 1b). This patient-age-specific selection was used as it is important to have as close as possible to a patient-specific boundary condition at the inlet. Additionally, the pressure gradient was set to zero at the inlet and the turbulent variables k and ω for the k-$\boldsymbol{\omega}$ SST model were calculated as recommended by Versteeg and Malalasekera (2007). For the k_T-k_L-$\boldsymbol{\omega}$ transition model, the values of k_T and ω were estimated similarly to the k-$\boldsymbol{\omega}$ SST model, while the value of k_L was set to zero, as established by Walters and Cokljat (2008).

At the outlets, a zero-gradient flux-corrected velocity boundary condition was imposed along with the zero-gradient condition for all turbulent quantities. Aditionally, pressure was set by a resistance boundary condition. In this case, the pressure varies according to the blood flow rate temporal profile but between healthy systolic and diastolic pressure levels, 120 mmHg and 80 mmHg, respectively, as recommended by Chnafa *et al.* (2018).A zero-gradient condition was also applied for the transitional and turbulent variables.

On the arterial and aneurysmal walls, suitable wall functions were used for k and ω for the k-$\boldsymbol{\omega}$ SST , while for the transition model, $k_L = k_T = 0$ and a zero-normal-gradient condition was applied for ω. The reasoning behind these boundary conditions is detailed in Walters and Cokljat (2008).

2.3 Computational Strategies

Both the laminar-flow equations and the turbulence equations were numerically solved using OpenFOAM®, version 22.12. To assure the second-order accuracy level, only second-order interpolation profiles were selected: the second-order upwind scheme for the advective term discretization with the Green-Gauss scheme for both velocity and pressure gradients discretizations and the second-order central differences for the surface-normal gradient in the diffusion terms with non-orthogonal and skew corrections (Jasak, 1996). The same discretization profiles were employed for the turbulent variables. The PISO algorithm (Issa, 1986) was used as the pressure-velocity coupling algorithm.

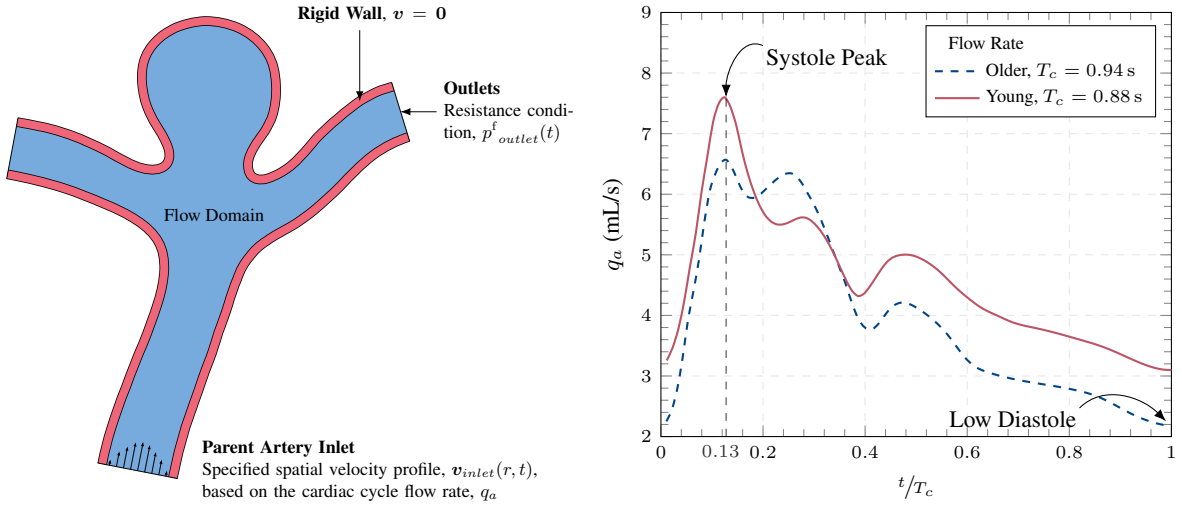

(a) (b)

Figure 1. (a) Schematic two-dimensional representation of a typical modeling applied to the flow in IAs with typical boundary conditions; (b) two blood flow rates waveforms that were be used at the inlet (time axis normalized by the cardiac period, T_c, of each profile.

The computational meshes were created using the utility `snappyHexMesh` of OpenFOAM®, which generates meshes that are dominantly composed of hexahedral cells. To fit the curved boundary, the cells near the wall are general polyhedra with a prismatic boundary-layer refinement composed of five layers. The structure of the mesh was created to provide systematically finer elements closer to the wall, instead of only the prismatic layer near the wall. For the turbulence modes simulations, the prismatic cells layers was refined to assured a sufficient y^+ near the wall to resolve the turbulent boundary layer. Mesh-sensitivity studies for the fluid meshes were carried out extensively with different IAs geometries and yielded a volume density of cells in the range of 3000 to 4000 cells/mm^3 (Oliveira *et al.*, 2021). Similarly, based on previous simulations performed for similar vascular geometries, a time-step of 1×10^{-4} s has been used. Three cardiac cycles were solved to avoid initial transient errors, but only the third one was analyzed in the results.

2.4 Data Analysis

We analyzed the magnitude of the WSS vector, $\boldsymbol{\tau}_w$, at the peak-systole instant (see Fig. 1b), represented by peak-systole WSS (PSWSS), and the time-averaged wall shear stress (TAWSS) field, defined as the time average of the magnitude of the $\boldsymbol{\tau}_w$ on the inner surface of the vessels, as follows:

$$TAWSS(\boldsymbol{x}) = \frac{1}{T_c}\int_0^{T_c} \|\boldsymbol{\tau}_w\| \mathrm{d}t \,, \tag{7}$$

and the OSI field (He and Ku, 1996), defined as:

$$OSI(\boldsymbol{x}) = \frac{1}{2}\left(1 - \frac{\left\|\frac{1}{T_c}\int_0^{T_c} \boldsymbol{\tau}_w(\boldsymbol{x},t)\mathrm{d}t\right\|}{\frac{1}{T_c}\int_0^{T_c} \|\boldsymbol{\tau}_w(\boldsymbol{x},t)\|\mathrm{d}t}\right) . \tag{8}$$

where T_c is the cardiac cycle period. The OSI varies between 0 and 0.5 and measures how the WSS vector varies over the cardiac cycle. Values closer to 0.5 indicate stagnant flow over the surface.

Additionally, the surface-average of each of the PSWSS, TAWSS, and the OSI fields was computed over the aneurysm surface, S_{ia}, of each case. For a field ϕ defined over the surface S_{ia}, with area A_{ia}, was computed as:

$$\langle\phi\rangle = \frac{1}{A(S_{ia})}\int_{S_{ia}} \phi(\boldsymbol{x})\mathrm{d}S_{ia} \,, \tag{9}$$

where the operator $A()$ gives the area of the surface S_{ia}.

3. RESULTS AND DISCUSSIONS

Figures 2 and 3 show the PSWSS and the OSI fields for the lateral aneurysm cases studied using the laminar flow model, the k-ω SST model, and the k_T-k_L-ω model. The first aneurysm case exhibits the typical flow behavior of lateral aneurysms, although with overall higher levels of PSWSS compared to the bifurcation aneurysm, as seen in Fig. 2. Typically, lateral aneurysms develop a recirculating flow within the aneurysm sac caused by a shearing zone at the aneurysm ostium, leading to lower levels of PSWSS and TAWSS, compared to bifurcation aneurysms. However, the higher values of PSWSS in this case are explained by higher velocities in the lateral aneurysm as this case involved a young patient and the bifurcation IA was from an older adult (see Fig. 1b). This is due to the formation of a slowly recirculating zone inside the aneurysm. Regarding the WSS, we observe that the use of different flow regimes assumptions do not influence the PSWSS, when the conditions are typically prone to transition. The figure shows that the k-ω SST model and the k_T-k_L-ω exhibit almost the same behavior as the laminar model. Similar results were found for the TAWSS, suggesting that, at least in these two IA cases, these trends occur for the complete cardiac cycle.

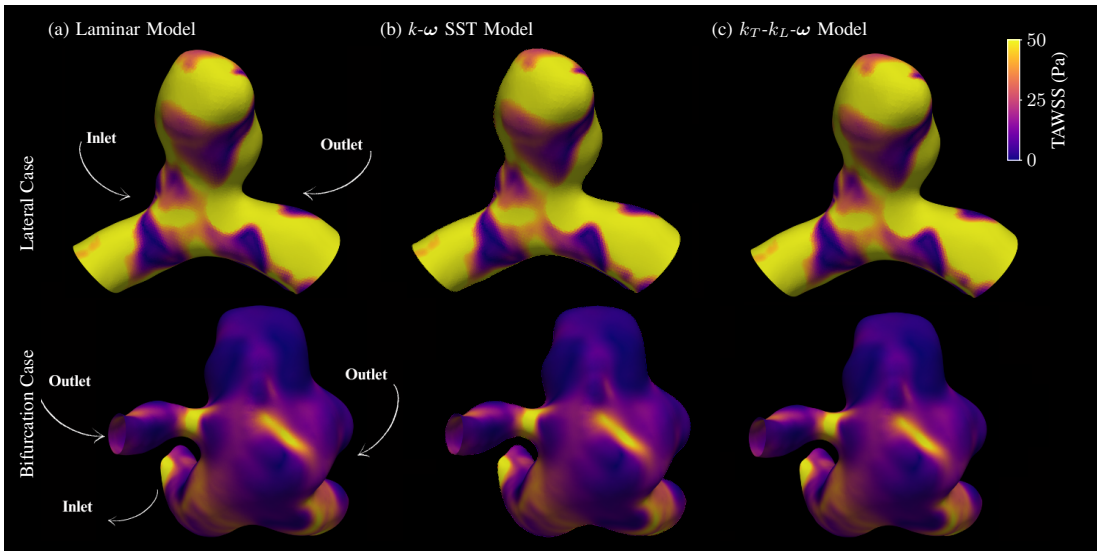

Figure 2. PSWSS field on the surface of both aneurysm cases for the (a) laminar model, (b) k-ω SST turbulence model and (c) the k_T-k_L-ω model.

Similar findings can be seen in the OSI field, as shown Fig. 3, where the patterns of OSI remain unaltered between the laminar and turbulent flows. This indicates that the local direction of the WSS vector is not influenced by the flow regime model either.

The similarities between the hemodynamics variables shown in Figs. 2 and 3 are confirmed by computing the surface-average of PSWSS and OSI on the aneurysm surface (see Table 1). Surprisingly, the largest differences occurred for the TAWSS in the lateral aneurysm case, which most likely indicates a difference between the flow patterns adjacent to the wall at instants after the peak systole. Furthermore, the k-ω SST and k_T-k_L-ω predict almost the same values, although the complexity of setting up the simulation case for the k_T-k_L-ω model is higher than for the k-ω SST model.

Table 1. Surface-averaged values over the aneurysm surface of the TAWSS, PSWSS and OSI fields of the lateral and bifurcation cases.

Case	Models	TAWSS (Pa)	PSWSS (Pa)	OSI
Lateral	Laminar	25.927	11.218	0.0083
	k-ω SST	26.152	11.223	0.0084
	k_T-k_L-ω	26.147	11.225	0.0084
Bifurcation	Laminar	5.189	0.624	0.0526
	k-ω SST	5.190	0.624	0.0540
	k_T-k_L-ω	5.186	0.626	0.0542

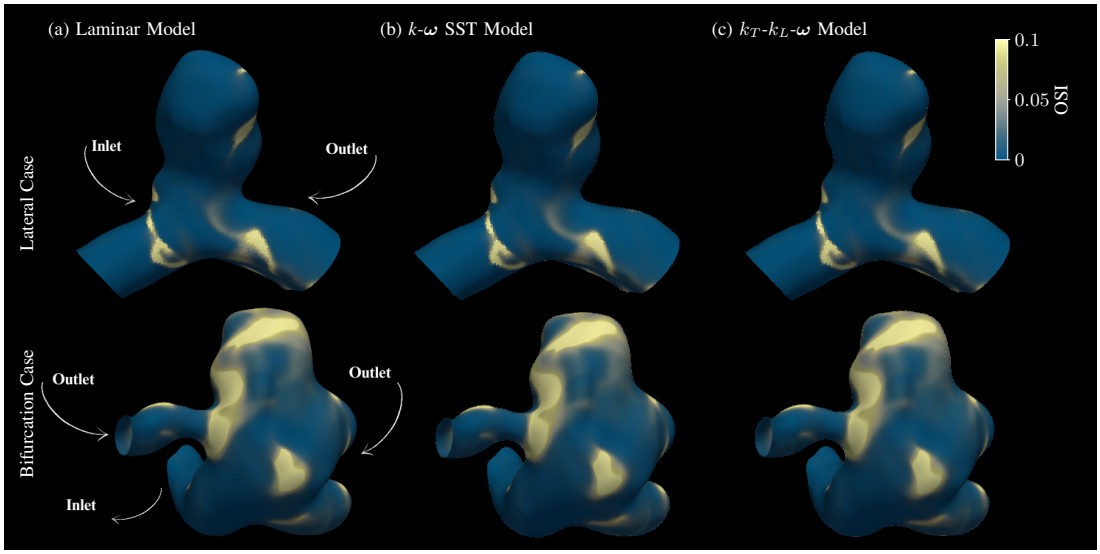

Figure 3. OSI field on the surface of both aneurysm cases for the (a) laminar model, (b) k-ω SST turbulence model and (c) the k_T-k_L-ω model.

To validate these results, we performed a laminar flow simulation with a highly-refined computational mesh (approximately 10 million cells, with a maximum cell size of approximately 0.5 mm) to investigate instabilities in the bifurcation aneurysm following the procedure used by Valen-Sendstad *et al.* (2011) that systematically refined the mesh up to values of mesh edge that were of the order of the Kolmogorov scales, thus using a DNS approach. This methodology has been applied elsewhere due to the low Reynolds number of aneurysmal flow. The results indicate unstable velocity patterns after the peak-systole by comparing the velocity magnitude at points located at the parent artery and the aneurysm sac (see Fig. 4).

These high-frequency velocity patterns inside the aneurysm suggest a transition to turbulence at the aneurysm entrance, as also recently investigated by Luciano *et al.* (2024). The authors investigated the energy cascade in the flow of IAs and their results suggest that, despite the low Reynolds numbers in the aneurysmal flow, the flow is turbulent around the aneurysm. Furthermore, according to our results for two aneurysm cases, although the velocities may exhibit unstable behavior similar to transition to turbulence, the instantaneous peak-systolic WSS is not influenced by using different turbulence or transition-to-turbulence flow models, nor are its time-average or derived quantities, such as the OSI.

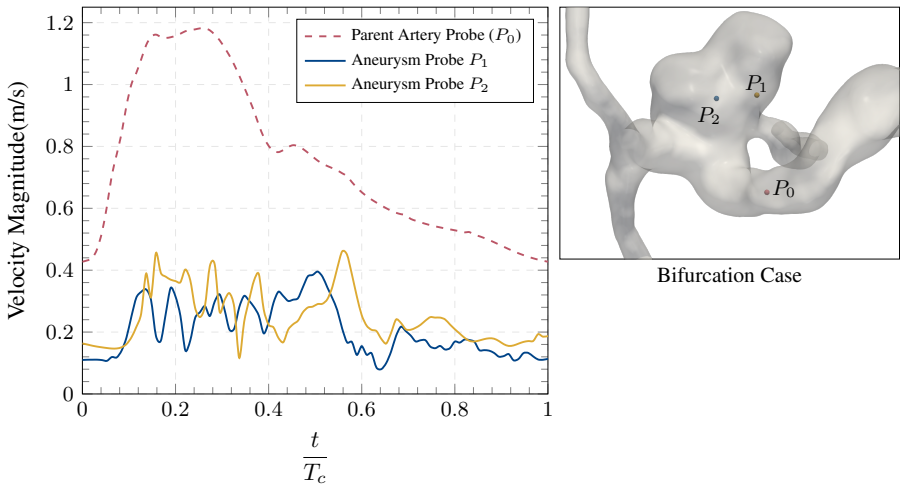

Figure 4. Velocity magnitude over the cardiac cycle at three probe locations of the bifurcation case run with a highly-refined mesh (probe locations shown at the picture on the right).

Limitations

The small sample size used in this study is a clear limitation, although we were careful to select cases that exhibited the flow features suggesting a transition to turbulence, according to the literature. Nonetheless, more cases should be simulated for a more comprehensive statistical analysis. Regarding the DNS results, we used the same interpolation profiles as described in Section 2.3 although it is recognized that these may be too diffusive for DNS simulations. Therefore, it is likely that the velocity waveforms shown in Fig. 4 from the probes inside the aneurysm sac exhibit higher-frequency instabilities.

4. CONCLUSIONS

Although several studies have found high-frequency instabilities in intracranial aneurysmal flow indicating transition to turbulence, our results suggest that modeling this flow with the k-ω SST , a typical turbulence model, or the k_T-k_L-ω model, employed for modeling transition to turbulence, does not alter the predictions of quantities that have been related to aneurysm rupture, such as the WSS and OSI. Therefore, if time-averaged quantities are especially required in a particular analysis, a laminar flow regime assumption may be sufficient. Nevertheless, further investigations of turbulent flow in intracranial aneurysms should be pursued, especially in the case of treated aneurysms. Endovascular treatment, for example, the most common one in IAs, involves medical devices such as stents that are braided-like structures prone to play an important role in the nature of IAs flow.

5. ACKNOWLEDGEMENTS

This research was supported by resources supplied by the Center for Scientific Computing (NCC/GridUNESP) of the São Paulo State University (UNESP) (`www2.unesp.br/portal#!/gridunesp`) and by the National Laboratory of Scientific Computing through the use of the SDumont supercomputer (project ID CFDIA). Funding: This research was supported by grants 2023/0771-1 and 2023/06609-9 of São Paulo Research Foundation (FAPESP).

6. REFERENCES

Cebral, J.R. and Meng, H., 2012. "Counterpoint: Realizing the Clinical Utility of Computational Fluid Dynamics—Closing the Gap". pp. 397–398. doi:10.3174/ajnr.a2993.

Chnafa, X.C., Brina, X.O., Pereira, V.M. and Steinman, X.D.A., 2018. "Better Than Nothing: A Rational Approach for Minimizing the Impact of Outflow Strategy on Cerebrovascular Simulations". Vol. 39, pp. 337–343. doi:10.3174/ajnr.A5484.

Ford, M.D., Alperin, N., Lee, S.H., Holdsworth, D.W. and Steinman, D.A., 2005. "Characterization of volumetric flow rate waveforms in the normal internal carotid and vertebral arteries". Vol. 26, No. 4, pp. 477–488. doi:10.1088/0967-3334/26/4/013.

He, X. and Ku, D.N., 1996. "Pulsatile Flow in the Human Left Coronary Artery Bifurcation: Average Conditions". Vol. 118, pp. 74–82. doi:10.1115/1.2795948.

Hoi, Y., Wasserman, B.A., Xie, Y.J., Najjar, S.S., Ferruci, L., Lakatta, E.G., Gerstenblith, G. and Steinman, D.A., 2010. "Characterization of volumetric flow rate waveforms at the carotid bifurcations of older adults". Vol. 31, No. 3, pp. 291–302. ISSN 09673334. doi:10.1088/0967-3334/31/3/002.

Isaksen, J.r.G., Bazilevs, Y., Kvamsdal, T., Zhang, Y., Kaspersen, J.H., Waterloo, K., Romner, B. and Ingebrigtsen, T., 2008. "Determination of wall tension in cerebral artery aneurysms by numerical simulation". Vol. 39, No. 12, pp. 3172–3178. ISSN 00392499. doi:10.1161/STROKEAHA.107.503698.

Issa, R.I., 1986. "Solution of the implicitly discretised fluid flow equations by operator-splitting". Vol. 62, No. 1, pp. 40–65. ISSN 10902716. doi:10.1016/0021-9991(86)90099-9.

Jain, K., Roller, S. and Mardal, K.A., 2016. "Transitional flow in intracranial aneurysms – A space and time refinement study below the Kolmogorov scales using Lattice Boltzmann Method". Vol. 127, pp. 36–46. ISSN 00457930. doi:10.1016/j.compfluid.2015.12.011.

Jasak, H., 1996. "Error Analysis and Estimation for the Finite Volume Method with Applications to Fluid Flows".

Kallmes, D.F., 2012. "Point: CFD—Computational Fluid Dynamics or Confounding Factor Dissemination". Vol. 33, pp. 393–398. doi:10.3174/ajnr.A2993.

Khan, M., Toro Arana, V., Najafi, M., MacDonald, D., Natarajan, T., Valen-Sendstad, K. and Steinman, D., 2021. "On the prevalence of flow instabilities from high-fidelity computational fluid dynamics of intracranial bifurcation aneurysms". Vol. 127, p. 110683. ISSN 00219290. doi:10.1016/j.jbiomech.2021.110683.

Liang, L., Steinman, D.A., Brina, O., Chnafa, C., Cancelliere, N.M. and Pereira, V.M., 2019. "Towards the Clinical utility

of CFD for assessment of intracranial aneurysm rupture - A systematic review and novel parameter-ranking tool". Vol. 11, pp. 153–158. ISSN 17598486. doi:10.1136/neurintsurg-2018-014246.

Luciano, R., Da Silva, B., Chen, X. and Bergstrom, D., 2024. "Turbulent blood flow in a cerebral artery with an aneurysm". Vol. 172, p. 112214. ISSN 00219290. doi:10.1016/j.jbiomech.2024.112214.

Oliveira, I.L., Santos, G.B., Militzer, J., Baccin, C.E., Tatit, R.T. and Gasche, J.L., 2021. "A longitudinal study of a lateral intracranial aneurysm: Identifying the hemodynamic parameters behind its inception and growth using computational fluid dynamics". Vol. 43, p. 138. doi:10.1007/s40430-021-02836-6.

Poelma, C., Watton, P.N. and Ventikos, Y., 2015. "Transitional flow in aneurysms and the computation of haemodynamic parameters". Vol. 12. doi:10.1098/rsif.2014.1394.

Saqr, K.M., Rashad, S., Tupin, S., Niizuma, K., Hassan, T., Tominaga, T. and Ohta, M., 2019. "What does computational fluid dynamics tell us about intracranial aneurysms? A meta-analysis and critical review". Vol. 0, No. 0, pp. 1–19. doi:10.1177/0271678X19854640.

Scotti, A. and Piomelli, U., 2002. "Turbulence Models in Pulsating Flows". Vol. 40, No. 3, pp. 537–544. ISSN 0001-1452, 1533-385X. doi:10.2514/2.1679.

Tupin, S., Saqr, K.M., Rashad, S., Niizuma, K. and Tominaga, T., 2020. "Non-Kolmogorov Turbulence and Inverse Energy Cascade in Intracranial Aneurysm: Near-Wall Scales Suggest Mechanobiological Relevance". URL `https://doi.org/10.48550/arXiv.2001.08234`.

Valen-Sendstad, K., Mardal, K.A., Mortensen, M., Reif, B.r.A.P. and Langtangen, H.P., 2011. "Direct numerical simulation of transitional flow in a patient-specific intracranial aneurysm". Vol. 44, pp. 2826–2832. doi:10.1016/j.jbiomech.2011.08.015.

Versteeg, H.K. and Malalasekera, W., 2007. *An Introduction to Computational Fluid Dynamics: The Finite Volume Method*. Pearson Education Ltd, 2nd edition. ISBN 978-0-13-127498-3.

Vlak, M.H.M., Rinkel, G.J.E., Greebe, P. and Algra, A., 2013. "Risk of rupture of an intracranial aneurysm based on patient characteristics: A case-control study". Vol. 44, No. 5, pp. 1256–1259. ISSN 00392499. doi:10.1161/STROKEAHA.111.000679.

Walters, D.K. and Cokljat, D., 2008. "A Three-Equation Eddy-Viscosity Model for Reynolds-Averaged Navier–Stokes Simulations of Transitional Flow". Vol. 130, No. 12, p. 121401. ISSN 0098-2202, 1528-901X. doi:10.1115/1.2979230.

Zarrinkoob, L., Ambarki, K., Wå hlin, A., Birgander, R., Eklund, A. and Malm, J., 2015. "Blood flow distribution in cerebral arteries". Vol. 35, pp. 648–654. ISSN 15597016. doi:10.1038/jcbfm.2014.241.

7. RESPONSIBILITY NOTICE

The authors are solely responsible for the printed material included in this paper.